HHS Public Access

Author manuscript

Faraday Discuss. Author manuscript; available in PMC 2019 January 02.

Published in final edited form as:

Faraday Discuss. 2016 October 06; 191: 351–372. doi:10.1039/c6fd00020g.

Anisotropic surface functionalization of Au nanorods driven by molecular architecture and curvature effects

Estefania Gonzalez Solveyra[¥], **Mario Tagliazucchi**[#], and **Igal Szleifer**[¥]

[¥]Department of Biomedical Engineering, Department of Chemistry and Chemistry of Life Processes Institute, Northwestern University.

[#]INQUIMAE-CONICET, DQIAyQF, Facultad de Ciencias Exactas y Naturales. Universidad de Buenos Aires.

Abstract

This work suggests a novel strategy to coat the caps and body of Au-nanorods (Au-NRs) with end-grafted polymer layers of different composition by taking advantage of the different curvature of these two regions. A molecular theory was used to theoretically investigate the effect of local curvature and molecular architecture (intramolecular connectivity of the monomers) on the adsorption of polymer mixtures on cylindrical (Au-NR body) and spherical (Au-NR caps) surfaces. The adsorption process was systematically studied as a function of the backbone length, number and position of branches, quality of the solvent and total number of monomers of the polymer molecules in the mixture. The balance between repulsive forces and polymer-surface and polymer-polymer attractions governs the amount and composition of the adsorbed layer. This balance is in turn modulated by the architecture of the polymers, the curvature of the surface and the competition between the different polymers in the mixture for the available area. As a result, the equilibrium composition of the polymer layer at spheres and cylinders of the same radius differs from each other, and in turn departs from that of the bulk solution. Curvature plays a major role: the available volume at a given distance from the surface is larger for spherical surfaces than for cylindrical ones, therefore the surface density of the bulkier (more branched) polymer in the mixture is larger on the Au-NR caps than on the Au-NR body. These results suggest that the combination of curvature at the nanoscale and tailored molecular architecture can confer anisotropic nanoparticles with spatially enriched domains and, therefore, lead to nanoconstructs with directional chemical interactions.

1) Introduction

Gold nanorods (Au-NRs) are great candidates for building multifunctional agents with anisotropic surface functionalization. In the past two decades, their unique electronic and optical properties, reproducible synthesis, stability, biosafety and ease of surface modification[1] have multiplied their applications in catalysis,[2] sensing and molecular

Supporting Information available

Molecular details of the polymers used in our calculations, figure showing the density and conformational properties of 20l-(35–2b) mixture on cylindrical surfaces, and additional figures expanding on the effects of the polymers' molecular architecture and the solvent quality on the adsorption process.

recognition,[3] and biomedical therapeutics and diagnosis.[4] The different curvatures of the bodies and the caps of Au-NRs offer a great opportunity to engineer anisotropic nanoconstructs. In such spatially heterogeneous NRs, both the location and the composition of the surface coating are important for their use in biomedical applications. The size, local geometry and orientation of the NRs at the contact point with cells play a crucial role in transport, delivery and cellular internalization.[5–7] Thus, controlling the chemistry and location on the NR surface of the grafted ligands can enable chemical directionality, with the ultimate goal of controlling interactions at the nano-bio interface.[8]

Surface modification is also key to modulate interactions at the interface of Au-NR and their surrounding media.[9] Following synthesis, Au-NRs must be functionalized with biocompatible molecules to prevent uncontrolled protein adsorption (biofouling) on the NRs' surface when introduced in biological matrices.[10] The most widely used antifouling ligands include poly(ethylene glycol) (PEG),[11] thiol self-assembled monolayers (SAMs),[12] zwitterionic polymers,[13] peptoids[14] and glycopeptoids.[15] Specific-targeting ligands, such as antibodies, proteins, nucleic acids or small ligands like sugars can also be incorporated to the Au-NRs in order to allow molecular recognition at the desired site.[16]

So far, significant progress has been achieved in anisotropic functionalization of Au NRs based on the distinct crystallographic faceting of their surface, since different crystallographic facets exhibit different chemical reactivity.[17,18] Subsequent functionalization with thiol-terminated molecules allows obtaining Au-NRs end-terminated with diverse ligands[17, 19–21] for applications in plasmonic metamaterials[22] and supracolloidal polymers.[23] However, in spite of the directionality incorporated in such strategies and the great control over the interparticle interactions, the as-modified Au-NRs in those works still present a CTAB bilayer along their longitudinal side, which poses serious problems for their utilization in biological and biomedical media.[4]

In this work, we propose to anisotropically modify Au-NRs by taking advantage of the different types of curvatures of their bodies and caps. For the adsorption of a single type of polymer type in solution, increasing the surface curvature (*i.e.* decreasing its radius) increases the amount of adsorbed polymer.[24, 25] This effect results from the fact that in curved convex surfaces, the available volume increases as the distance from the surface increases, and it scales as (r/R) for cylinders and as $(r/R)^2$ for spheres (where r is the radial direction and R the radius of the surface). Based on this fact, we hypothesize that in a system combining both cylindrical and spherical surfaces, such as an idealized NR (see Figure 1b), surface curvature can be used for spatially selective functionalization. In order to explore this hypothesis, we study the adsorption of mixtures of a linear and a branched polymer (with varying degree of branching) in order to improve partitioning of the branched polymers between caps and body and maximize the effect of curvature, as schematically shown in Figure 1a. Keeping in mind the intended purpose of designing Au-NRs for biomedical applications, the polymers explored in this work are neutral and hydrophilic, as numerous publications have reported that hydrophobic or charged coatings tend to adsorb more proteins than neutral or hydrophilic surfaces.[26, 27]

In the next section, we present the theory for polymer adsorption from binary solutions on curved surfaces. All polymers studied in this work adsorb on the surface exclusively through a functional end group. Then, we present a discussion of the effect of different variables on the adsorption process: composition of the solution, radius of the NR, the molecular architecture of the polymer molecules and solvent quality. In the last section, we outline the design rules that resulted from our study and discuss the potentials of the methodology employed.

2) Theoretical Methods

In order to model the adsorption of polymer mixtures on the surface of the NRs, we independently study the adsorption on the spherical caps and the cylindrical body (Figure 1b). We consider a curved surface (either cylindrical or spherical) in contact with aqueous solutions containing a mixture of two polymer molecules with different molecular topology. We model the adsorption of the end group of these polymers on the cylindrical and spherical surfaces with typical radius, R, from 1 to 20 nm, as depicted in Figure 1b–c.

2.1) Molecular theory

Our theoretical approach is based on a molecular theory developed to describe a wide range of soft-matter phenomena at interfaces, including the structure and thermodynamics of tethered polymer layers,[24, 28] the adsorption of polymer and proteins,[14, 29–31] ligand-receptor binding,[32–35] acid-base equilibrium of weak polyelectrolytes grafted on surfaces of different curvature[36–38] and interfacial behavior of diverse nanomaterials.[39–41] The predictive power of the molecular theory on the behavior of soft matter in a variety of systems (as compared with experiments[42–47]) gives us confidence about its potential to outline design rules in the synthesis of anisotropically coated NRs.

The employed theory explicitly considers the geometry of the system, the shape, molecular volume and conformations of all molecular species and the repulsive excluded-volume and attractive Van der Waals (VdW) interactions. The input of the theory is a set of conformations for each macromolecule in the system and the values of the controlled thermodynamic variables (temperature, composition of the bulk solution, adsorption energy, etc.). Minimization of the system's free energy yields structural and thermodynamic properties of the system at equilibrium, including the probability of each conformation, the amount of adsorbed polymer and the spatial distribution of solvent molecules and polymer chains.

The starting point of the theory is an approximate free-energy functional for the system. We are studying a surface in contact with an aqueous solution having a constant composition of linear (l) and branched (b) polymers (we also assume that the composition of the solution is unaffected by adsorption), therefore the calculations have to be performed in the grand canonical ensemble. The grand potential per unit area can be expressed as:

$$\frac{\beta W}{A} = \sum_{i=l,\ b} \sigma_i \sum_{\{\alpha_i\}} P(\alpha_i)\ln P(\alpha_i) + \sum_{i=l,b} \sigma_i[\ln(\sigma_i \Lambda_i^2) - 1] \quad \text{(Eq. 1)}$$

$$+ \sum_{i=l,\ b} \sigma_i \beta \epsilon_s - \sum_{i=l,\ b} \sigma_i \beta \mu_i^{bulk}$$

$$+ \int d\mathbf{r} \quad \rho_w(\mathbf{r})[ln(\rho_w(\mathbf{r}) v_w) - 1]$$

$$+ \frac{\beta}{2} \iint d\mathbf{r} \quad d\mathbf{r}' \frac{\chi \quad a(|\mathbf{r} - \mathbf{r}'|)}{v_p} \left[\left\langle \phi_p^l(\mathbf{r}) \right\rangle + \quad \left\langle \phi_p^b(\mathbf{r}) \right\rangle\right] [\left\langle \phi_p^l(\mathbf{r}') \right\rangle + \quad \left\langle \phi_p^b(\mathbf{r}') \right\rangle]$$

with $\beta = 1/k_B T$ (k_B is the Boltzmann constant, T is the absolute temperature) and $\mathbf{r}$ is the position vector, $\mathbf{r} = (x, y, z)$. The amount of adsorbed polymer is quantified through its surface density $\sigma_i = N_i/A(R)$ where N_i is the number of adsorbed molecules of the linear or branched polymer, $A(R)$ corresponds to the area and R to the radius of curvature of the surface, which can be planar ($R \rightarrow \infty$), cylindrical or spherical.

The first term in Eq. 1 corresponds to the conformational entropy of the polymer chains, where $P(\alpha_i)$ (with $i = l$ *or* b) is the probability of having a linear or branched polymer molecule tethered to the surface in a conformational state α. The second term is the two-dimensional (surface) translational entropy of the polymers, where $\Lambda_i = (h^2/2\pi m_i k_B T)^{1/2}$ is the polymer de Broglie wavelength, h is Planck's constant and m_i is the polymer molecular mass. The third term corresponds to the adsorption energy between the end-segment of the polymer chain and the surface, with ϵ_s being the adsorption energy per chain. The fourth term ensures that the chemical potential of each type of polymer, μ_i^{bulk}, is the same at the surface and in the bulk solution. The fifth term is the translational (mixing) entropy of the water molecules, where $\rho_w(\mathbf{r})$ is the position-dependent water density and v_w is the molecular volume of a water molecule. The last term is the VdW effective attractive energy between polymer segments.[24] In this term, $\left\langle \phi_p^i(\mathbf{r}) \right\rangle$ is the volume fraction of the polymer at $\mathbf{r}$ (with $i = l$ *or* b), χ is a prefactor that determines the strength of the polymer-polymer interaction and $a(|\mathbf{r} - \mathbf{r}'|)$ is a distance-dependent VdW attractive function of the form:

$$a(|\mathbf{r} - \mathbf{r}'|) = -\left(\frac{l_{seg}}{|\mathbf{r} - \mathbf{r}'|}\right)^6 \text{for} l_{seg} \quad |\mathbf{r} - \mathbf{r}'| < 1.5\delta \quad \text{(Eq. 2)}$$

$$a(|\mathbf{r} - \mathbf{r}'|) = \quad 0 \text{otherwise}$$

with l_{seg} being the segment length and 1.5δ a cut-off parameter (δ is the discretization step, see below).

The repulsion between molecules is accounted for by an incompressibility condition ensuring that the total available volume is occupied either by the polymers or solvent molecules at all distances from the surface:

$$\left\langle \phi_p^l(\mathbf{r}) \right\rangle + \left\langle \phi_p^b(\mathbf{r}) \right\rangle + \phi_w(\mathbf{r}) = 1 \quad \text{(Eq. 3)}$$

where $\phi_w(\mathbf{r})$ is the position-dependent volume fraction of water and $\left\langle \phi_p^i(\mathbf{r}) \right\rangle$ are the position-dependent volume fractions of the polymer (for i = l, b), given by:

$$\left\langle \phi_p^i(\mathbf{r}) \right\rangle = \sigma_i \sum_{\{\alpha_i\}} P(\alpha_i) n(\alpha_i; \mathbf{r}) \quad \text{(Eq. 4)}$$

where $n(\alpha_i; \mathbf{r})d\mathbf{r}$ is the number of segments that the chain in conformation α_i has within the volume between $\mathbf{r}$ and $\mathbf{r} + d\mathbf{r}$.

The system's free energy is a functional of $\phi_w(\mathbf{r})$, $P(\alpha_i)$, and σ_i. These quantities are found by the minimization of Eq. 1 subject to the packing constraint (Eq. 3), introducing a set of Lagrange multipliers $\beta\pi(\mathbf{r})$. This procedure yields:

$$\phi_w(\mathbf{r}) = \rho_w(\mathbf{r}) v_w = \exp[-\beta\pi(\mathbf{r}) v_w] \quad \text{(Eq. 5)}$$

for the solvent density, and:

$$P(\alpha_i) = \frac{1}{q_i} \exp\left\{ -\int \beta\pi(\mathbf{r}) v_p \; n(\alpha_i; \mathbf{r}) d\mathbf{r} - \iint d\mathbf{r} \; d\mathbf{r}' \; \chi \; a(|\mathbf{r} - \mathbf{r}'|) n(\alpha_i; \mathbf{r}) [\left\langle \phi_p^l(\mathbf{r}') \right\rangle + \left\langle \phi_p^b(\mathbf{r}') \right\rangle] \right\}$$

(Eq. 6)

for the probability of chain conformations, where $i = l$ *or* b, q_i is a normalization constant assuring $\sum_{\{\alpha_i\}} P(\alpha_i) = 1$ and v_p is the volume of a monomer.

Minimization with respect to surface coverage gives:

$$\sigma_i = \frac{q_i}{\Lambda_i^2} \exp[\beta\mu_i^{bulk} - \beta\epsilon_s] \quad \text{(Eq. 7)}$$

This equation guarantees that the chemical potential of the linear or branched polymer molecules ($i = l$ *or* b) on the surface (μ_i^{surf}) is the same as in the bulk solution (μ_i^{bulk}), as required by thermodynamic equilibrium.

The only unknowns in the above equations are the position-dependent repulsive interactions $\pi(\mathbf{r})$, which correspond to the osmotic pressure along the system.[24, 36] They are determined by replacing the expressions for $P(\alpha_i)$, σ_i, and $\phi_w(\mathbf{r})$ into the packing constraint (Eq.3). To implement the theory, we exploit the cylindrical or spherical symmetry of the system by adopting the corresponding coordinates system in our calculations.[35, 36] Furthermore, we assume that the system is laterally homogeneous, with the inhomogeneities explicitly considered only in the radial direction. Thus, we change our variable from $\mathbf{r}$ to r, and define r as the distance from the surface (*i.e.* r is the radial coordinate for a cylinder or sphere). For each specific geometry, we discretize the space in layers of dimension δ, transforming the integral equation for $\pi(r)$ into a set of nonlinear equations that we solve by standard numerical methods. For further details on solving the theory we refer the interested reader to refs.[36, 48]

2.2) Molecular model

In order to solve the theory, we need sets of chain conformations for the linear and branched polymers. While these sets include in principle all allowed conformations that do not collide with the surface for the geometry under study, in practice it is enough to use a very large set of randomly chosen conformations, which we generate in free space using the rotational-isomeric model (RIS).[49] To avoid biases, each random bond sequence is rotated using randomly chosen Euler angles.[50] Only self-avoiding conformations that do not overlap with the surface are considered. We have used a set of 10^6 different configurations for each polymer type and each geometry.

To study the effect of the bulk solution composition, we varied the molar fraction of the branched polymer (x_b^{bulk}) in a mixture of branched and linear polymers between zero (solution of linear polymer only) and one (solution of branched polymer only). For all cases, we kept the total volume fraction of polymer constant ($\phi_{p_l}^{bulk} + \phi_{p_b}^{bulk} = \phi_{p_{tot}}^{bulk} = 0.015$). For each composition of the solution, we computed the bulk chemical potential of the polymers (μ_i^{bulk}) within the same theoretical approach as that of the tethered chains described above, following the expression:[24]

$$\beta\mu_i^{bulk} = -\ln(N_i^{bulk}) - \frac{v_p}{v_w} n_{seg_i} \ln\phi_w^{bulk} + \ln\left(\frac{\phi_{p_i}^{bulk}}{n_{seg_i}}\right) + \beta \quad \chi \quad a \quad n_{seg_i}\phi_{p_i}^{bulk} \qquad \text{(Eq. 8)}$$

where $i = l$ *or* b, N_i^{bulk} is the total number of self-avoiding conformations for each type of polymer and n_{seg_i} is the total number of segments in the chain. All the other quantities have been defined above. Note that since the bulk solution is an homogeneous system, the

attractive function a corresponds simply to $a = \iint d\mathbf{r}\, d\mathbf{r}'\, a(|\mathbf{r} - \mathbf{r}'|)$, and that ϕ_i are the volume fractions of species $i = p^l, p^b, w$ for the linear, branched polymers and water in the solution respectively, with $\phi_w^{bulk} + \phi_{p_l}^{bulk} + \phi_{p_b}^{bulk} = 1$.

We chose the parameters for the monomers of the polymer to be that of PEG (segment length l_{seg} = 0.3nm and segment volume v_p = 0.065nm^3) based on a previous implementation of the molecular theory.[28] The solvent molecular volume was set to 0.03 nm^3 (based on water's density) and the thickness of the discrete layers to δ = 0.3 nm. The adsorption energy of the functionalized end group (ϵ_s) for all polymers considered in this work was set to −13.2 k_BT in order to reproduce the experimental surface density obtained for the adsorption of a 20-monomer linear chain on a planar surface, obtained experimentally in a previous work.[14] We conducted calculations considering different values of $\frac{\chi_c}{\chi}$, where χ_c is the critical parameter defined as the value required to induce microphase segregation in a neutral polymer layer in the limit of vanishing surface coverage[51] and it is close to Θ conditions.[52] Values of $\frac{\chi_c}{\chi}$ greater and lower than 1 correspond to good and poor solvent conditions, respectively.

Using the theory and molecular model described above, we performed a systematic analysis on the adsorption process varying the backbone length, number of branches, branching positions, total number of monomers in the polymer molecules (see Figure 1c) and quality of the solvent. In particular, we are interested in exploring routes that would allow enriching the spherical caps with the branched polymers. The number and position of the branches have been selected given the interest in having a large density of free ends close to the solvent for further chemical. Details of the chains can be found in Table S1 in the ESI.

3) Results and discussion

We start our analysis discussing polymer adsorption from mixtures in good solvent conditions. We reserve the discussion of polymer-polymer interactions and the role of solvent quality on the adsorption process for the last section of our results. It is worth mentioning that we allow adsorption only between the end segment of the polymer and the Au-NR. We do not consider mechanisms encompassing backbone- and branch-mediated adsorption. For detailed studies of such systems, including polymer architecture effects, we refer the reader to Ref[53] and references therein.

The nomenclature used henceforth for the different polymer chains comprise the total number of segments in the molecule, followed by the number of branches. In the case of linear polymers, the code we use is simply the number of segments followed by the letter "l", for "linear". So, "20l" corresponds to a linear polymer of 20 monomers, while "35–2b" corresponds to a branched polymer of 35 total monomers, and 2 branches. Note that for all branched polymers, the number of segments on the branches is the same and equal to 5 (see Table S1 in the ESI).

3.1) Single-polymer solutions

The thermodynamic behavior of polymers adsorbing on surfaces is intimately related to the molecular organization of the chains at the grafting surface. Carignano and Szleifer have previously addressed the conformational properties of linear and branched polymers on surfaces of planar, cylindrical, and spherical geometry,[24] and also provided a detailed analysis on the adsorption of linear chains on curved surfaces.[24, 48] So, we focus our discussion on the interplay of chain architecture and polymer adsorption in systems containing only one type of polymer as an introduction for the polymer adsorption from binary mixtures in the following sections.

Figure 2a shows the equilibrium amount of polymer adsorbed as a function of the radius of the surface, for both cylinders and spheres. The amount of adsorbed polymer results from the balance between competing processes, modulated by the curvature of the surface: the attractive forces between the polymer functionalized end segment and the surface, the loss of conformational entropy induced by packing the chains at the surface and the excluded volume repulsions between the monomers that are confined to the surface vicinity. It is worth recalling that in all the cases studied, the attraction between the end group of the polymer and the surface is the same for all molecules. Hence, the difference in adsorption derives from the entropic repulsive contributions.

The adsorption isotherms for the different polymers on the same geometry and radius in Figure 2a, reflect that the repulsions depend very strongly on the shape and size of the molecules. Increasing the molecular weight of the polymers (*i.e.* total number of segments), leads to an increase in the steric repulsion within the adsorbed layer and, therefore, to a decrease of the adsorbed density (35l vs. 20l). The intrinsic effect of the molecular topology is reflected on the adsorption of 35l vs. 35–2b, where the only difference is the arrangement of the monomers in the chain. The branched chain is bulkier than the linear one; hence, in the good solvent regime under discussion, it experiences stronger intramolecular repulsions and reaches a lower grafting density at equilibrium than the linear polymer.

Regarding the effect of the surface curvature, we observe that the adsorption increases as the radius of the curvature of the surface decreases, irrespective of the molecular topology or the morphology of the surface. This is due to the fact that in curved convex surfaces, the available volume increases as the distance from the surface increases, scaling as (r/R) for cylinders and as $(r/R)^2$ for spheres (where r is the radial direction and R the radius of the surface). This decreases the steric repulsions within the layer, giving rise to a greater adsorption on spheres than on a cylindrical geometry with the same radius. In a NR, which has spherical caps and cylindrical body, curvature leads to denser films on the caps than on the body. Therefore, the partition between the caps and body (which we define as the ratio of the equilibrium surface densities on the sphere and the cylinder, $\sigma_{sph}/\sigma_{cyl}$) is always larger than one (Figure 2b). Long polymer chains adsorb preferentially in regions with large available volume and, therefore, they have larger sphere/cylinder partition than short polymers, as observed by comparing 20l and 35l in Figure 2b. However, we do not observe large partition differences between linear and branched polymers, when comparing 35l and 35–3b in Figure 2b.

Based on these results, we will focus on the possibility of using mixtures of polymer chains with different molecular topology in order to enhance the curvature-driven partition. This effect can be useful to engineer surface-modified nanomaterials where different types of molecules enable multifunctional platforms.

3.2) Polymer adsorption from binary mixtures: combining molecular topology and surface curvature

3.2.1) General description of adsorption—Figure 3a shows the equilibrium amount of linear and branched polymers adsorbed as a function of the bulk composition of the solution for spherical surfaces, for a binary mixture of polymers comprising the polymers 20l and 35–2b. We show the results for $R = 1$ nm, but they are representative of the qualitative behavior in the other systems studied.

The adsorption isotherms demonstrate the complexity in the balance of forces that determine adsorption: the attraction between the end-segment of the polymers and the surface, the repulsive interactions between adsorbed molecules and the entropy of mixing. There is a monotonic decrease (increase) in the adsorbed amount of the linear (branched) polymer, as the solution becomes more concentrated in the branched polymer. However, the linear polymer 20l is the major component of the adsorbed film until the solution has 80% of the branched polymer. The preferential adsorption of 20l over 35–2b is due to excluded-volume interactions, since the short linear polymer can accommodate better than the long branched one in the proximity of the surface. The fraction of the branched polymer in solution that leads to a layer with 50% of branched polymer is very sensitive to the molecular details of the polymer chains and to the relative difference in size and shape between the linear and the branched chains.

The effect of bulk composition on the overall adsorption is also shown in Figure 3a. We observe that the total amount of adsorbed polymers, $\sigma_{TOT} = \sigma_l + \sigma_b$, is a monotonic decreasing function of the bulk composition for the branched polymer.

The interplay between curvature, molecular architecture and bulk composition is reflected in the curvature-driven partition (Figure 3b). The sphere/cylinder partition is always larger for the branched polymer than for the linear one due to the bulkier nature of the branched chains. This drives its partition towards the sphere, demonstrating the possibility of enriching the spherical end of a NR with the bulkier polymer in the mixture. The sphere/cylinder partition for both the linear and branched polymers decreases monotonically with the content of branched polymer in solution. As x_b^{bulk} increases, the competition between the flexible linear chains and the bulky branched ones hinders the adsorption of the linear polymer on regions of larger available volume and, thus, the sphere/cylinder partition for the linear polymer decreases. Regarding the branched polymer, the adsorbed amount on both surfaces increases with increasing bulk concentration (Figure 3a), but this increase, relative to the maximum surface density at $x_b^{bulk} = 1$, is higher on the cylinder than on the sphere. Thus, the occupancy of the available surface increases faster with x_b^{bulk} for the cylinder than for the sphere and the branched polymer partition towards the sphere decreases for increasing x_b^{bulk}. Also, we observe that the partition for the branched polymer does not depend very strongly with the composition of the solution, which could be of interest when

engineering nanomaterials for diverse applications as it would allow maximizing the surface density by adjusting the bulk solution without significantly affecting the spatial partition. It is interesting to note that for the limiting value of $x_b^{bulk} \sim 1$, the decrease in the curvature-induced partition for the linear polymer falls below 1. While for the adsorption of a single type of polymer in good solvent, the partition should be always be larger than one, there exists conditions where the partition of one of the polymers in a mixture falls below one (*i.e.* that polymer is enriched at the surface of the cylindrical body in comparison with the spherical tip). The effect results from the fact that adsorption of mixtures is a competition for the available surface area; therefore, one of the polymers may strongly adsorb, thus depleting the other one from the spherical surface and making its sphere/cylinder partition smaller than one. Changing the quality of the solvent can enhance this effect further, as we discuss below.

The differences in available volume for each geometry dictates the molecular organization of the layer and defines the amount of adsorption for each polymer. The conformational properties of the layer strongly depend on the architecture of the chains. The variation of the polymer volume fraction as a function of the distance from the tethering surface accounts for the interplay between curvature and molecular architecture, as shown in Figure 3c. It is worth noting that the density profiles depend on the grafting density, and that this quantity in turns changes for each geometry (Figure S1). Increasing the fraction of branched polymer in solution increases the amount of the branched polymer on the surface, and with that the steric repulsions in the layer. The system lowers these repulsions by the combination of two mechanisms: i) stretching both the linear and branched chains towards regions of greater available volume (at the cost of conformational entropy) and ii) decreasing the total amount of adsorbed polymer (at the cost of decreasing the total adsorption energy, Figure 3a).

The results from our calculations show that the composition of the surface-adsorbed layer departs strongly from the bulk composition for all the geometries studied, as shown in Figure 4. Moreover, in curved surfaces of increasing radius, the composition of the adsorbed mixture tends to that of the planar surface. The composition of the branched polymer in the bulk required to obtain a 1:1 mixture on the surface ($x_b^{surf} = 0.5$) is always larger than 0.5 and shifts to higher values as the radius of the surface increases (Figure 4b). In the limit of highly curved surfaces, ($R = 1$ nm, Figure 4a), we observe that for a solution with $x_b^{surf} = 0.9$ the surface fraction of the branched polymer on the sphere is 60% whereas for a cylinder of the same radius is 35%. This result strongly suggests the possibility of enriching the adsorbed mixture in the branched polymer in surfaces of high curvature.

3.2.2) Molecular architecture effects—We now provide an analysis of the effect of the number of branches, the branching positions, the backbone length and the topology of the polymer molecules on the competitive adsorption of binary polymer mixtures on surfaces of different geometry. Due to the complexity of the system, the effect of these variables is highly non-additive (see below). Thus, we will not attempt to analyze all possible combinations of these different variables, but rather focus our efforts in systematically analyze combinations that can improve the partition of the branched polymer toward the Au-NR tips. Given the dimensions of commonly synthetized Au-NRs,[4] we will study systems of 5 nm radius.

Branching Effect: Figure 5 shows the effect of increasing the number of branches at constant backbone length of the branched polymer. In all cases, the linear polymer corresponds to the polymer 20l. The branched polymer has a backbone of 20 segments, and one, two, or three branches. We observed that the surface density of branched polymer systematically decreases with increasing number of branches (Figure 5a). This is due to the increase in the size and bulkiness of the branched polymer, which results in an increase of the steric repulsions that hinder adsorption in good solvent conditions. This in turns favors the adsorption of the linear polymer (Figure 5a), yielding an overall adsorption ($\sigma_{tot} = \sigma_b + \sigma_l$) that decreases slightly with increasing number of branches at constant backbone length, both on spheres and cylinders (Figure 5b). One could, therefore, optimize the molecular structure of the chains in the mixtures without compromising the total amount of adsorbed polymer (σ_{tot}), which can be very beneficial when engineering materials for biological applications. The increasing crowding near the surface with increasing number of branches at constant backbone length also results in a more favorable partition of the branched polymer towards the regions of higher curvature (Figure 5c). The linear polymer in the mixture is also preferentially partitioned towards the sphere (Figure S2) although to a much lesser extent than the branched polymers. For both the branched and the linear polymer, the partition is maximal for $x_b^{bulk} = 0$ (*i.e.* pure linear polymer solution), as we discussed above.

The effect of increasing the number of branches on polymer adsorption depends strongly on the length of the backbone of the branched polymer. Figure S3 shows the analysis for mixtures comprising the same linear polymer as in Figure 5, but branched polymers with 35 monomers in the backbone instead of 20, with varying number of branches. The qualitative effects are the same as discussed above, but much less dramatic, and become even less important for branched polymers of even longer backbones (data not shown). The position of the branches along the polymer backbone is also very important. Figure 6 shows the surface density of each individual polymer in mixtures comprising the same linear polymer of 20 segments and branched chains containing three branches in different positions with respect to the surface. It can be appreciated that short branches near the surface are very detrimental for the adsorption process of the branched polymer, favoring the adsorption of the linear polymer in almost all the range of bulk solution composition. Increasing the spacing between the position of the first branch and the surface strongly favors its adsorption, despite the increase in the total number of monomers. This behavior depends on the number of branches of the polymer, as we discuss below.

Backbone length effect: In this section we explore the effect of changing the backbone length of the branched polymers for a constant number of branches (the length of the backbone changes below the position of the first branch), see scheme in Figure 7. Increasing the backbone length for the one-branch polymer decreases the surface density of the branched polymer and increases that of the linear chain (Figure 7a). On the other hand, when the branched polymer has three branches, increasing the backbone length increases the amount of the adsorbed branched polymer and decreases that of the linear chain (Figure 7b). Mixtures containing two-branch chains show a behavior intermediate between the one-branch and the three-branch polymers (Figure S4).

The molecular organization of the adsorbed layer is the result of the balancing forces governing the adsorption process. In the case of the one-branch polymers, where the branching point is near the end of the chain (Table S1 in the ESI and scheme in Figure 7), the repulsive forces with neighboring molecules result in stretched configurations, in which the branch orients towards the solution (Figure S5). So, their behavior is similar to that of a linear polymer. In this scenario, increasing the backbone of the branched chain does not significantly modify the region of the chain that competes for the available volume with the short linear chain near the surface. On the other hand, in the three-branch polymers, the short branches cannot be accommodated in a way that resembles a linear chain (see Figures 8 and S6). When the backbones of the linear and the branched polymers have similar length, there is a competition for the available space between the linear chain and the much bulkier branched chain. However, when the backbone of the branched chain is longer than the linear chain, the competition for the available volume occurs between the linear chain and a region of the linear backbone of the branched chain. This last scenario also improves the accessibility of the free-end segments from the solution. Figure 8 shows the density of free ends as a function of the distance from the surface. This quantity reflects the most probable position of the free-end segments for the polymers in the mixture. It can be seen that making the backbone of the branched chain longer than the linear polymer allows for the free ends of the branched polymer to be located towards the solution. On the other hand, in branched chains with a short 20-segment backbone, the free ends remain buried within the layer and, thus, inaccessible from solution (Figure S6). The concern about accessibility of free ends is of prime importance for conferring further chemical functionalities to these segments for improved biotargeting or tailored chemical reactivity of the nanoconstruct.

The effects of the molecular architecture of the polymers (backbone length and number of branches) on the curvature-induced partition are summarized in Figure 9, where we show the ratio between the surface density on spheres and cylinders of radius 5 (panel a) and 1 nm (panel b) for mixtures of a 20-segment linear polymer (20l) with branched polymers with different backbone length and number of branches. The bulk composition plotted, x_b^{bulk} = 0.9, was chosen to have a significant amount of adsorbed branched polymer. In general, the partition between spheres and cylinders increases when increasing the number of branches or the backbone length. The outlier behavior of the three-branch polymer with a backbone of 20 segments derives from the strong repulsions with the linear polymer, as we discussed above. It is worth keeping in mind that in that case, the total adsorbed amount of polymer is significantly diminished, so there is a compromise between achieving a curvature-induced partition and reaching an appropriate surface density. While the partition for R = 5 nm, which is in the range of usual sizes of NRs for biomedical applications,[4] is rather large, it is possible to increase it further by increasing the curvature of the surface, see results for R = 1 nm in Figure 9b.

The strategies we discussed so far were targeted towards favoring a partition of the branched polymer to spherical surfaces with respect to cylinders of equivalent radius. It is worth mentioning that different partition scenarios are possible based on the molecular architecture of the chains. For example, in binary mixtures comprising a linear chain longer than the backbone of the branched polymer, we observed that these long linear chains end up partitioning to the regions of greater curvature, *i.e.* away from the surface (Figure S7).

Molecular topology: Strategically combining the molecular architecture for each chain could allow tuning the competitive adsorption of the molecules on surfaces of different curvature. But, now we ask: What is the gain in resorting to a mixture of a linear and a branched chains instead of mixtures of two linear polymers of different lengths? To that end, we analyzed the differences between a mixture comprising a linear polymer of 20 monomers (20l) and a three-branch polymer of 50 monomers total (50–3b), and a mixture comprising the same linear polymer (20l) and another linear polymer of 50 monomers (50l). Note that the polymers 50–3b and 50l have exactly the same number of monomers, but different topology. We observed that the surface density of 50–3b is slightly smaller than that of 50l (Figure 10a), which results from the fact that the first branching position of 50–3b is at segment 24, while the length of the 20l polymer is 20 segments (see scheme in Figure 10). Therefore, the 50–3b polymer experiences greater steric repulsions than the 50l, hindering its adsorption. In the case of the 20l+50l mixture, competition for the available space between linear chains results in a more favorable adsorption than for the mixture 20l+(50–3b). However, the curvature-induced partition between spherical and cylindrical surfaces is similar for both mixtures (Figure 10b). We also observed this behavior for the adsorption of polymers of equal number of total monomers from solutions containing one single polymer type (Figure 2b, 35l vs. 35–2b). The end-segment accessibility from the solution for the 50–3b polymer (Figure 10-c, **upper panel**) is more hindered by the linear 20l polymer than for the 50l chains (Figure 10-c, **lower panel**), but the overall accessibility is rather good in both cases. Thus, resorting to a branched polymer instead of a linear polymer of the same number of total monomers results is an increase in the density and accessibility of available end-segments, but with a small decrease in amount of adsorbed polymers. Once again, this behavior is strongly dependent on the branching positions of the polymer, for instance a 3-branch chain with two branches points below the end-backbone of the linear chain (Figure S8) shows a smaller surface density at equilibrium and less accessible free ends than those reported for the branched polymer in Figure 10. As a conclusion, we propose a general design rule: in order to optimize polymer adsorption and free end accessibility, the length of the backbone between the surface-bound segment and the first branching position in the branched chain should be longer than the length of the linear polymer.

3.2.3) Role of polymer-polymer interactions—

The results presented so far corresponded to polymer mixtures in good solvent (*i.e.* $\frac{\chi_c}{\chi} = \infty$, where higher $\frac{\chi_c}{\chi}$ correspond to better solvent quality). To address the role of the solvent quality in the competitive polymer adsorption process, we analyzed the adsorption from a binary polymer mixture considering values of $\frac{\chi_c}{\chi}$ equal to ∞, 1.43 and 0.83 (Figure 11). Note that the parameter $\frac{\chi_c}{\chi}$ is a proxy for the reduced temperature of the system, i.e the polymer is in a good solvent for $\frac{\chi_c}{\chi} > 1$ and in a poor solvent for $\frac{\chi_c}{\chi} < 1$. The parameter $\frac{\chi_c}{\chi}$ results from normalizing the strength of segment-segment attractions, χ, by the critical value χ_c (computed in a separate set of calculations), which is defined as the value of χ required to trigger microphase separation for a neutral, planar polymer brush in the limit of vanishing surface coverage.[52, 54] It is worth to mention that all the polymer mixtures studied here are

thermodynamically stable as homogeneous solutions, *i.e.* for the moderate poor solvents conditions that we use, the bulk solution does not phase separate.

As the quality of the solvent decreases, we observe that polymer adsorption increases, due to the higher attractive forces between monomers in the polymers with respect to the solvent. This increase in the amount of adsorbed changes dramatically when $\frac{\chi_c}{\chi} < 1$ (Figure 11a). At the same time, the fraction of the branched polymer in the adsorbed layer increases because this polymer has a greater number of segments than the linear one (35 vs. 20) and, therefore, experiences stronger polymer-polymer attractions that compete with the steric repulsions. Interestingly, while the quality of the solvent affects the amount and composition of the adsorbed polymer layer, it has little effect on the curvature-induced partition between spheres and cylinders for $R = 5$ nm (Figure 11c). It is also worth noticing that the curvature-induced partition for the linear polymer falls below 1 for high values of x_b^{bulk} (Figure 11c). This is due to the fact that the partition results from the competition between both types of polymers for the available surface area and, therefore, it can become smaller than one for a given polymer if the other polymer in the mixture adsorbs strongly to the spherical surface, blocking it, as discussed above.

Finally, we observed little qualitative differences on the effect of the molecular architecture of the polymer chains in the competitive adsorption process when decreasing the quality of the solvent. As discussed in the above paragraph, there is a change in the adsorbed amount, the surface composition and the curvature-induced for each value of $\frac{\chi_c}{\chi}$, but the trends we observed for the good solvent conditions regarding branching and backbone effects, do not show significant changes (Figure S9).

4) Conclusions

In the present work, we propose a novel strategy to construct gold nanorods with chemically inhomogeneous coatings by using the different curvature of the tips and the body to direct the adsorption of the components of a polymer mixture. To test this strategy, we analyzed the effect of surface curvature and molecular topology on polymer adsorption from binary solutions on Au NR modeled as the combination of spherical and cylindrical surfaces, representing the tips and body of the NR, respectively. Our calculations suggest that a spatially resolved surface modification could be attainable by adjusting the surface curvature, the molecular architecture of polymer chains, and the concentration of the bulk solution. Combining polymers of different architecture introduces a competition between them for the available surface. A complex balance between repulsive forces and polymer-surface and polymer-polymer attractions, modulated by the underlying curvature, governs the overall adsorption process. The composition of the surface mixture departs strongly from that of the bulk solution, and it depends on the curvature, morphology and specific details of the polymers in the mixture. We observed a curvature-induced partition between spherical and cylindrical surfaces that strongly depends on the radius of the curved surface, but can be adjusted by tailoring the molecular topology of the chains in the mixture. For the smallest dimensions of Au-NRs reported in the literature ($R = 5$nm),[1, 2] the enrichment effect for the

branched polymer in the mixture is typically a factor of 1.5–2 (*i.e.* we predict the adsorption of approximately twice the amount of branched polymer on the Au-NR tip than on its body). This effect can be further increased to factors of 4–5 for $R = 1$ nm (Figure 9a), which may be achievable with nanoparticles with very sharp tips such as Au nanostars[55] or with semiconductor NRs, whose diameters can be controlled in the few-nm range.[56] Another possible route to increase the curvature-induced partition is to use Au nano-dumbbells,[47] whose body has a concave curvature and, therefore, exhibits a smaller available volume near the surface than the cylindrical body of Au NRs.

The strength of the theoretical strategy employed in this work lies in the explicit description of the different competing interactions, while taking full advantage of the symmetry of the system in order to reduce the computational cost of the calculations. Our methodology allowed us to perform a systematic analysis of the relevant parameters on polymer adsorption from binary mixtures, which included calculations on over 100 different polymer mixtures in 50 solutions of different compositions and solvent qualities. This type of systematic analysis would be out of reach using Molecular Dynamics computer simulations, which are currently limited to study a few cases.[57] Our methodology also allowed us to ask questions about structure-property relationships that are very hard to observe experimentally. Particularly, we can outline some useful design rules that would lead to a partition of the branched polymer towards regions of higher curvature:

- The positions of the branching points are crucial: short branches near the surface have a drastic negative effect on the adsorption of the branched polymer, so in order to optimize the adsorption of the branched polymer, the length of the chain segment between the surface and the position of the first branch for a branched polymer should be larger than the length of the linear chain,
- Increasing the number of branches at constant backbone length decreases the adsorbed amount, but at the same time, it favors the partition between sphere and cylinders
- Using mildly poor solvent conditions allows increasing the amount of adsorbed branched polymer without drastically decreasing the sphere/cylinder partition.

Future work will encompass modeling systems that simultaneously combine surfaces of different curvature the NRs in two dimensions, which would allow us to explore Au NRs of different aspect ratios as well as nanoparticle shapes beyond Au NRs, such as nano-dumbbells.

Supplementary Material

Refer to Web version on PubMed Central for supplementary material.

Acknowledgments

This research was supported by Grant No. EB005772 from the National Institute of Biomedical Imaging and Bio-engineering (NIBIB). MT is a fellow of CONICET (Argentina). The authors greatly appreciate the assistance of Ingrid Goobar-Szleifer during the writing of the manuscript.

References

1. Li N, Zhao P and Astruc D, Angew. Chem. Int. Ed, 2014, 53, 1756–1789.
2. Pérez-Juste J, Pastoriza-Santos I, Liz-Marzán LM and Mulvaney P, Coordination Chemistry Reviews, 2005, 249, 1870–1901.
3. Huang X, El-Sayed IH, Qian W and El-Sayed MA, J. Am. Chem. Soc, 2006, 128, 2115–2120. [PubMed: 16464114]
4. Dreaden EC, Alkilany AM, Huang X, Murphy CJ and El-Sayed MA, Chem. Soc. Rev, 2012, 41, 2740–2779. [PubMed: 22109657]
5. Champion JA and Mitragotri S, Proc. Natl. Acad. Sci. U.S.A, 2006, 103, 4930–4934. [PubMed: 16549762]
6. Shi X, von dem Bussche A, Hurt RH, Kane AB and Gao H, Nature Nanotechnology, 2011, 6, 714–719.
7. Vácha R, Martinez-Veracoechea FJ and Frenkel D, Nano Letters, 2011, 11, 5391–5395. [PubMed: 22047641]
8. Lee C, Lee WB and Kang T, Applied Physics Letters, 2013, 103, 091602.
9. Gonzalez Solveyra E and Szleifer I, Wiley Interdisciplinary Reviews: Nanomedicine and Nanobiotechnology, 2015, DOI: 10.1002/wnan.1365.
10. Palui G, Aldeek F, Wang W and Mattoussi H, Chem. Soc. Rev, 2015, 44, 193–227. [PubMed: 25029116]
11. Lu HB, Campbell CT and Castner DG, Langmuir, 2000, 16, 1711–1718.
12. Harder P, Grunze M, Dahint R, Whitesides GM and Laibinis PE, The Journal of Physical Chemistry B, 1998, 102, 426–436.
13. Lau KHA, Sileika TS, Park SH, Sousa AML, Burch P, Szleifer I and Messersmith PB, Adv. Mater. Interfaces, 2015, 2, 1400225–1400235. [PubMed: 26167449]
14. Lau KHA, Ren C, Park SH, Szleifer I and Messersmith PB, Langmuir, 2012, 28, 2288–2298. [PubMed: 22107438]
15. Ham HO, Park SH, Kurutz JW, Szleifer IG and Messersmith PB, J. Am. Chem. Soc, 2013, 135, 13015–13022. [PubMed: 23919653]
16. Sapsford KE, Algar WR, Berti L, Gemmill KB, Casey BJ, Oh E, Stewart MH and Medintz IL, Chemical Reviews, 2013, 113, 1904–2074. [PubMed: 23432378]
17. Caswell KK, Wilson JN, Bunz UHF and Murphy CJ, J. Am. Chem. Soc, 2003, 125, 13914–13915. [PubMed: 14611200]
18. Murphy CJ, Thompson LB, Alkilany AM, Sisco PN, Boulos SP, Sivapalan ST, Yang JA, Chernak DJ and Huang J, The Journal of Physical Chemistry Letters, 2010, 1, 2867–2875.
19. Nie Z, Fava D, Kumacheva E, Zou S, Walker GC and Rubinstein M, Nature Materials, 2007, 6, 609–614. [PubMed: 17618291]
20. Nie, Fava D, Rubinstein M and Kumacheva E, J. Am. Chem. Soc, 2008, 130, 3683–3689. [PubMed: 18298120]
21. Fava D, Winnik MA and Kumacheva E, Chemical Communications, 2009, 2571–2573. [PubMed: 19532893]
22. Mühlig S, Cunningham A, Dintinger J, Scharf T, Bürgi T, Lederer F and Rockstuhl C, Nanophotonics, 2013, 2, 211–240.
23. Lukach A, Liu K, Therien-Aubin H and Kumacheva E, J. Am. Chem. Soc, 2012, 134, 18853–18859. [PubMed: 23078101]
24. Szleifer I and Carignano MA, Adv. Chem. Phys, 1996, 94, 165–260.
25. Walkey CD, Olsen JB, Guo H, Emili A and Chan WCW, J. Am. Chem. Soc, 2012, 134, 2139–2147. [PubMed: 22191645]
26. Lundqvist M, Stigler J, Elia G, Lynch I, Cedervall T and Dawson KA, Proceedings of the National Academy of Sciences, 2008, 105, 14265–14270.
27. Walkey CD, Olsen JB, Song F, Liu R, Guo H, Olsen DWH, Cohen Y, Emili A and Chan WCW, ACS Nano, 2014, 8, 2439–2455. [PubMed: 24517450]

28. Szleifer I, Current Opinion in Colloid & Interface Science, 1996, 1, 416–423.
29. Fang and Szleifer I, Langmuir, 2002, 18, 5497–5510.
30. Szleifer I, Biophysj, 1997, 72, 595–612.
31. Szleifer I, Physica A: Statistical Mechanics and its Applications, 1997, 244, 370–388.
32. Longo G and Szleifer I, Langmuir, 2005, 21, 11342–11351. [PubMed: 16285809]
33. Longo GS, Thompson DH and Szleifer I, Langmuir, 2008, 24, 10324–10333. [PubMed: 18698869]
34. Nap RJ and Szleifer I, Biomater. Sci, 2013, 1, 814–823. [PubMed: 23930222]
35. Tagliazucchi M and Szleifer I, J. Am. Chem. Soc, 2015, 137, 12539–12551. [PubMed: 26368839]
36. Nap R, Gong P and Szleifer I, J. Polym. Sci. B Polym. Phys, 2006, 44, 2638–2662.
37. Nap RJ, Božič AL, Szleifer I and Podgornik R, Biophysj, 2014, 107, 1970–1979.
38. Wang D, Nap RJ, Lagzi I. n., Kowalczyk B, Han S, Grzybowski BA and Szleifer I, J. Am. Chem. Soc, 2011, 133, 2192–2197. [PubMed: 21280574]
39. Nap RJ, Park SH and Szleifer I, J. Polym. Sci. B Polym. Phys, 2014, 52, 1689–1699.
40. Shvartzman-Cohen R, Nativ-Roth E, Baskaran E, Levi-Kalisman Y, Szleifer I and Yerushalmi-Rozen R, J. Am. Chem. Soc, 2004, 126, 14850–14857. [PubMed: 15535711]
41. Tagliazucchi M and Szleifer I, Soft Matter, 2012, 8, 7292.
42. Andrieu-Brunsen A, Micoureau S, Tagliazucchi M, Szleifer I, Azzaroni O and Soler-Illia G. J. d. A. A., Chem. Mater, 2015, 27, 808–821.
43. Ren C.-l., Carvajal D, Shull KR and Szleifer I, Langmuir, 2009, 25, 12283–12292. [PubMed: 19821628]
44. Tagliazucchi M, Azzaroni O and Szleifer I, J. Am. Chem. Soc, 2010, 132, 12404–12411. [PubMed: 20718436]
45. Tagliazucchi M, Calvo EJ and Szleifer I, Langmuir, 2008, 24, 2869–2877. [PubMed: 18251557]
46. Tagliazucchi M, Calvo EJ and Szleifer I, J. Phys. Chem. C, 2008, 112, 458–471.
47. Walker DA, Leitsch EK, Nap RJ, Szleifer I and Grzybowski BA, Nature Nanotechnology, 2013, 8, 676–681.
48. Carignano MA and Szleifer I, J Chem Phys, 1995, 102, 8662–8669.
49. Flory PJ, Statistical mechanics of chain molecules, Interscience Publishers, New York, 1969.
50. Carignano MA and Szleifer I, J Chem Phys, 1993, 98, 5006–5018.
51. Tagliazucchi M, de la Cruz MO and Szleifer I, Proceedings of the National Academy of Sciences, 2010, 107, 5300–5305.
52. Gong P, Genzer J and Szleifer I, Phys. Rev. Lett, 2007, 98, 018302. [PubMed: 17358511]
53. Naderi A, Iruthayaraj J, Pettersson T. r., Makuška R. a. and Claesson PM, Langmuir, 2008, 24, 6676–6682. [PubMed: 18512871]
54. Peleg O, Tagliazucchi M, Kröger M, Rabin Y and Szleifer I, ACS Nano, 2011, 5, 4737–4747. [PubMed: 21524134]
55. Dam DHM, Lee JH, Sisco PN, Co DT, Zhang M, Wasielewski MR and Odom TW, ACS Nano, 2012, 6, 3318–3326. [PubMed: 22424173]
56. Tice DB, Weinberg DJ, Mathew N, Chang RPH and Weiss EA, J. Phys. Chem. C, 2013, 117, 13289–13296.
57. Donakowski MD, Godbe JM, Sknepnek R, Knowles KE, de la Cruz M. Olvera and Weiss EA, J. Phys. Chem. C, 2010, 114, 22526–22534.

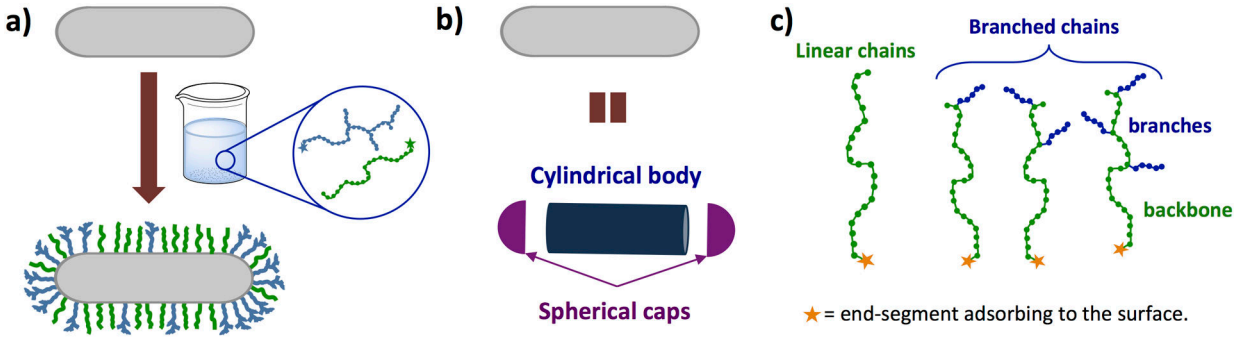

Figure 1:

Modeling strategy. **a)** Spatially heterogeneous surface-functionalized nanorod (NR) prepared by adsorbing a mixture of polymers of different molecular architecture from aqueous solution (Scheme not to scale). **b)** Schematic representation of a NR as a combination of surfaces of different curvature: cylinders and spheres, representing the NR's body and caps respectively. **c)** Schematic representation of the polymer architectures and relevant parameters analyzed in this work.

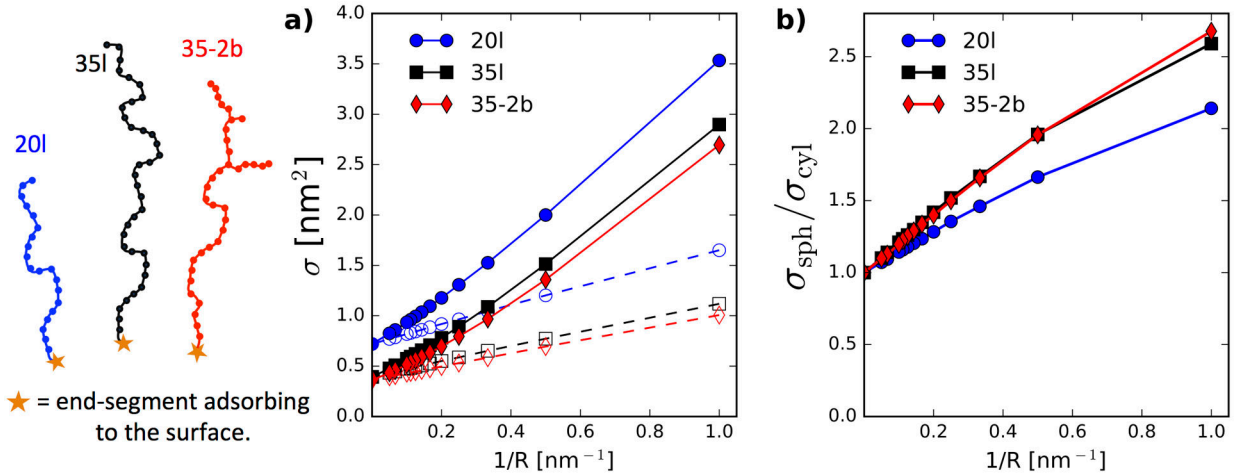

Figure 2: Curvature effect on polymer adsorption from one-polymer solutions.

a) Equilibrium surface coverage of adsorbed polymer as a function of the curvature for spherical (full lines and solid symbols) and cylindrical (dashed lines and empty symbols) surfaces. Results correspond to the adsorption from aqueous solutions containing one type of polymer of different architecture (blue and circle symbols: linear polymer of 20 monomers, 20l; black and square symbols: linear polymer of 35 monomers, 35l; red and diamond symbols: branched polymer of 35 total monomers, 25 segments in the backbone and 2 branches of 5 segments each, 35–2b). **b)** Partition between spheres and cylinders as a function of radius, for the same mixtures as in panel a.

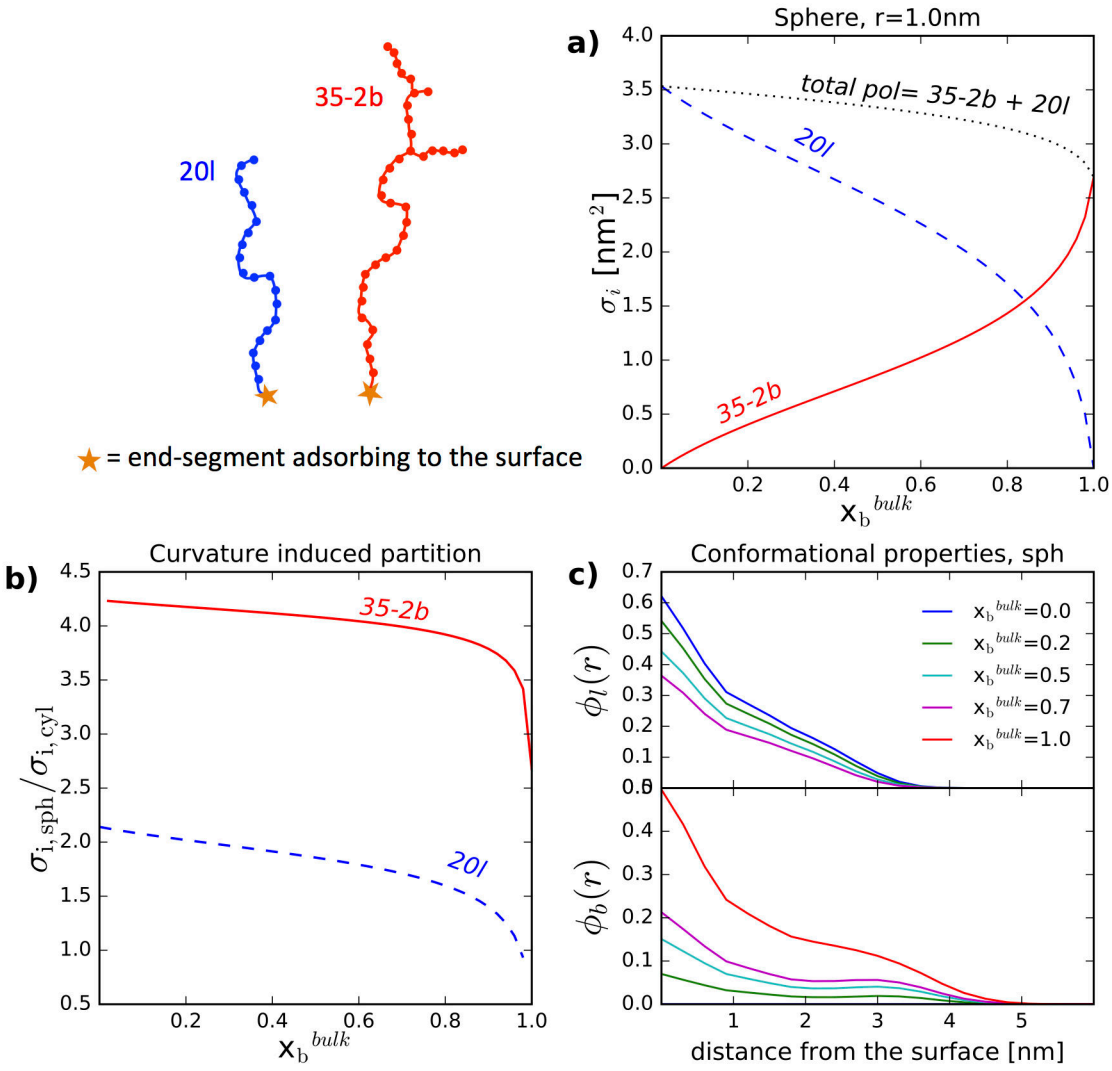

Figure 3:

a) Density of surface adsorbed polymers as a function of the molar fraction of the branched polymer in the bulk for a mixture comprising a linear polymer of 20 monomers (20l, blue line dashed) and a branched polymer of 35 total monomers, 25 segments in the backbone and 2 branches (35–2b, red solid line) on a sphere or R = 1 nm (see scheme on the left). **b)** Partition of the linear, the branched and the total amount of polymer between a sphere and a cylinder of 1 nm radius. Colors and lines as in panel a. **c)** Volume fraction of the adsorbed mixture as a function of the distance from the tethering surface. Results correspond to a spherical surface of radius 1 nm. Upper and lower graphs correspond to the volume fraction of the linear and the branched polymer, respectively. Colors correspond to different composition of the bulk solution, as indicated in the legend.

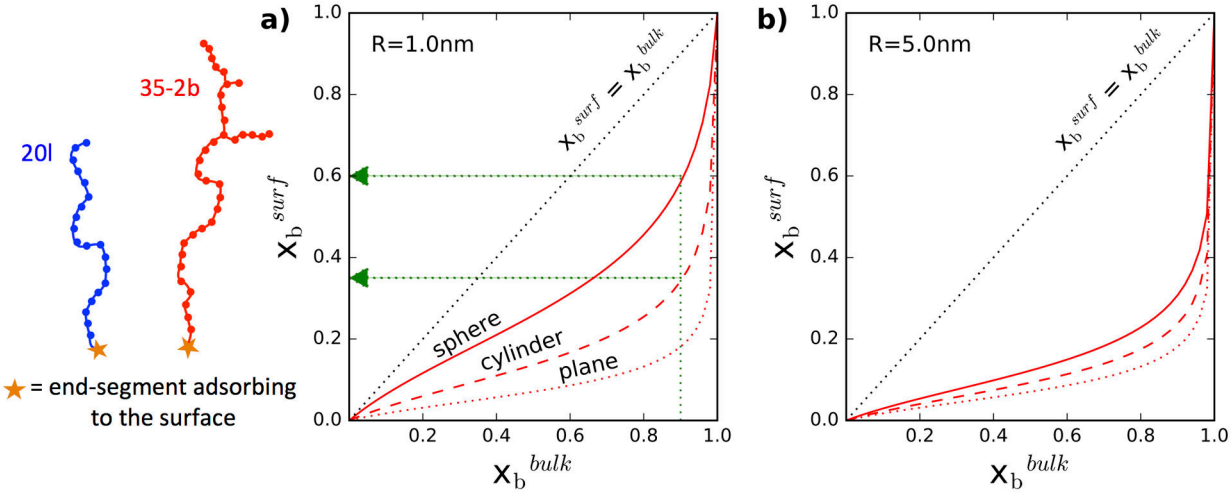

Figure 4:

Composition of the surface-adsorbed mixture as a function of the molar fraction of the branched polymer in the bulk for different geometries and curvatures. Results correspond to a mixture comprising a linear polymer of 20 monomers (20l) and a branched polymer of 35 total monomers, 25 segments in the backbone and 2 branched (35–2b, see scheme on the left) **a)** Full, dashed and dotted red lines correspond to a spherical, cylindrical, and planar surfaces respectively. Black dotted line corresponds to a surface composition equal to that of the bulk solution. Green dotted arrow indicate the partitioning for a solution with x_b^{bulk}= 0.9: the surface fraction of the branched polymer on a sphere of R = 1 nm is ~ 60% whereas for a cylinder of the same radius is ~ 35%. **b)** Same as panel a, but R = 5 nm for curved surfaces.

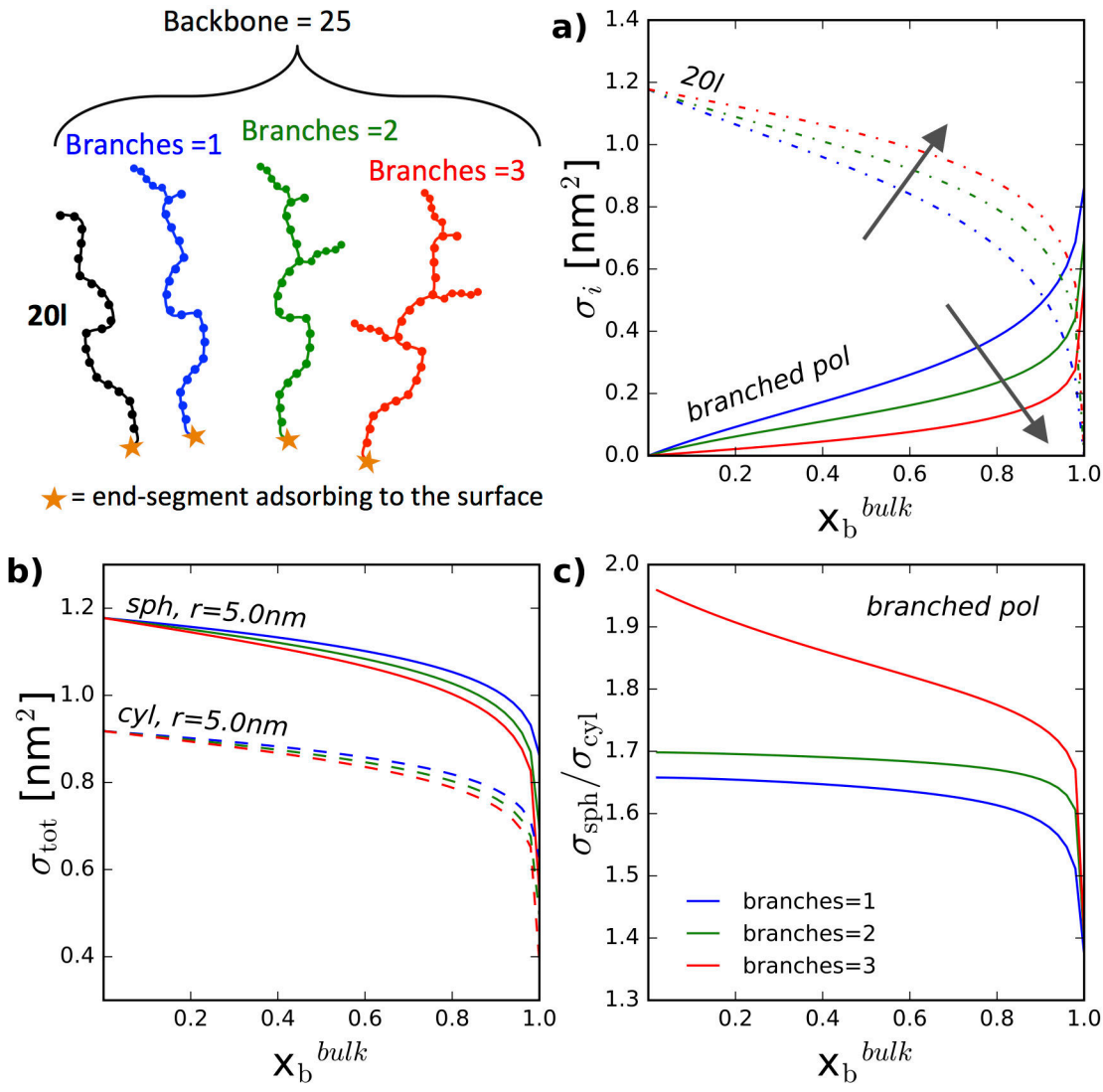

Figure 5:

Effect of polymer branching on the adsorption for polymer mixtures comprising a linear polymer of 20 monomers (20l) and a branched polymer with backbone length = 25 segments and one, two or three branches (colors blue, green, and red respectively, as shown in panel c, and in scheme on the upper left panel). All results correspond to curved surfaces of R = 5nm. **a)** Surface density of the adsorbed linear (dash-dot lines) and branched polymer (full lines) as a function of the bulk molar fraction of the branched polymer for a spherical surface**. b)** Total surface density of adsorbed polymers ($\sigma_{tot} = \sigma_l + \sigma_b$) as a function of the bulk molar fraction of the branched polymer for spherical (full lines) and cylindrical (dashed lines) surfaces. **c)** Sphere-cylinder partition for the branched polymer in the mixture as a function of the bulk molar fraction of the branched polymer.

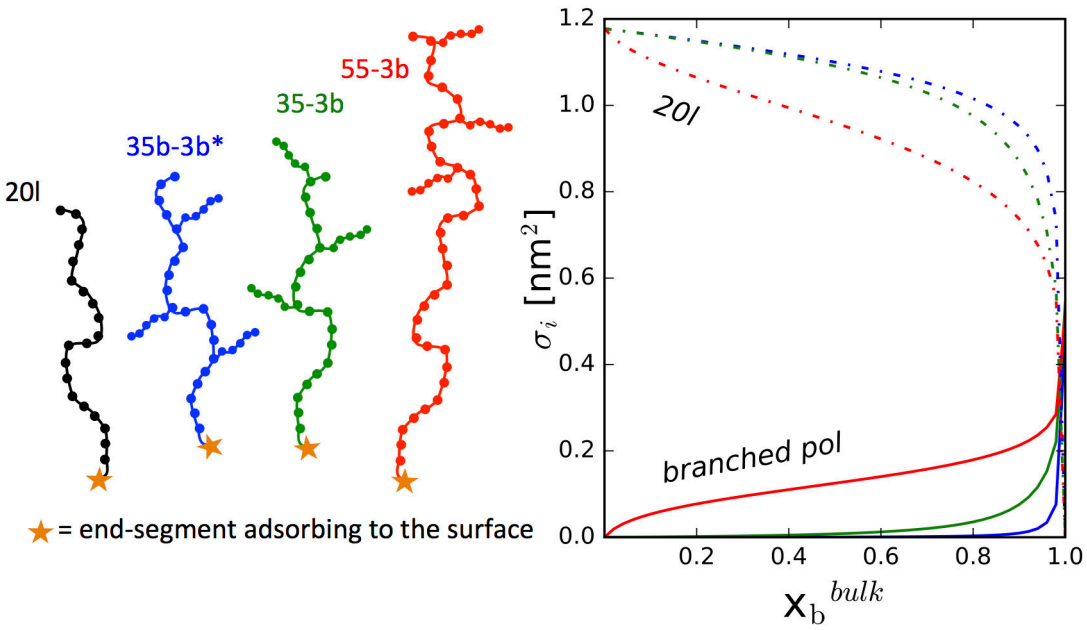

Figure 6:

Effect of the position of the branches with respect to the surface on the adsorption for polymer mixtures comprising a linear polymer of 20 monomers and the branched polymers depicted in the scheme, on a spherical surface of R = 5nm. The surface densities of the adsorbed linear (dash-dot lines) and branched polymers (full lines) are plotted as a function of the bulk molar fraction of the branched polymer. The colors of the lines are the same as those in the scheme.

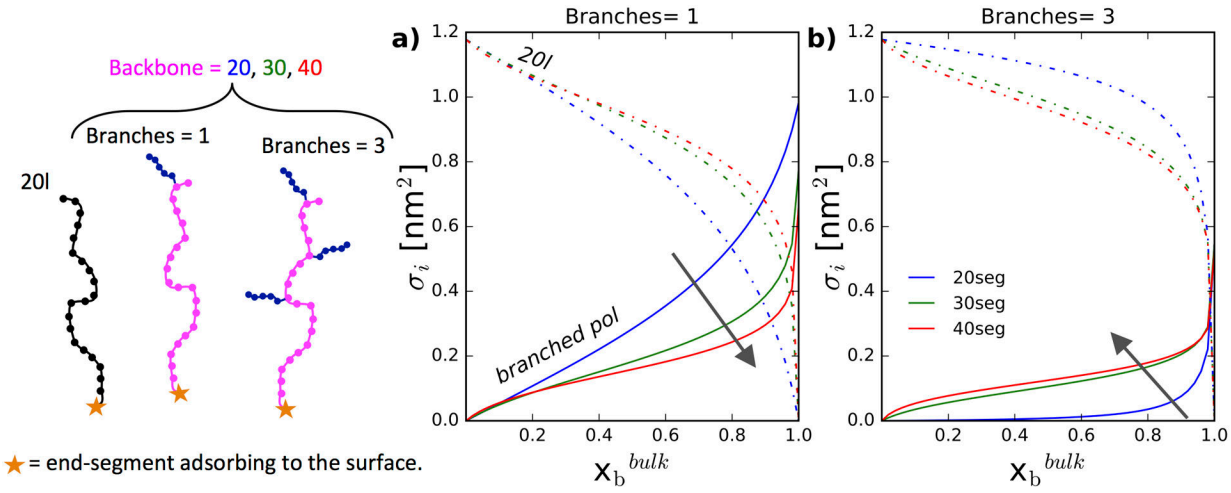

Figure 7:

a-b) Surface density of adsorbed polymers as a function of the bulk molar fraction of the branched polymer for mixtures comprising a linear (20l, dash-dot lines) and a branched polymer (full lines) with different backbone length (20, 30, 40 monomers in blue, green, and red lines respectively) and containing either one or three branches (see scheme on the left). Results correspond to a spherical surface of $R = 5$ nm.

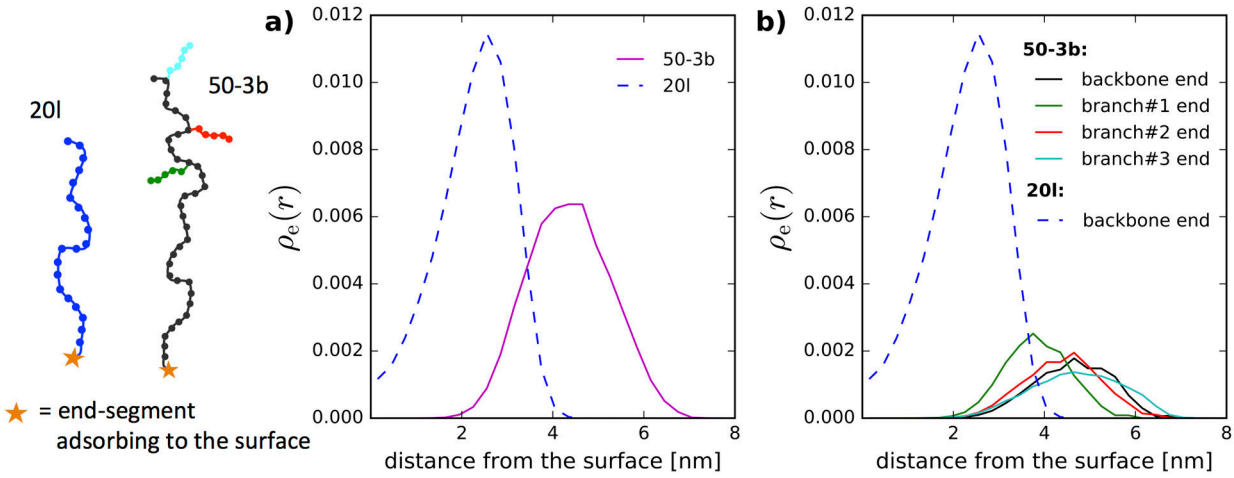

Figure 8:

Density of free ends as a function of the distance from the tethering surface for a spherical surface of $R = 5$ nm. Plots correspond to a mixture of a linear polymer of 20 monomers (20l) and a branched polymer with 3 branches and backbone length of 35 segments (50–3b, see scheme on the left). All the cases are for a fixed bulk composition with $x_b^{bulk} = 0.9$. Dashed lines show the end-segment density of the backbone of the linear polymer (panels **a** and **b**). Full lines show the sum of the end-segment densities of the backbone and each branch of the branched polymer in panel **a** and a detail of the individual densities of each type of end segment in panel **b**.

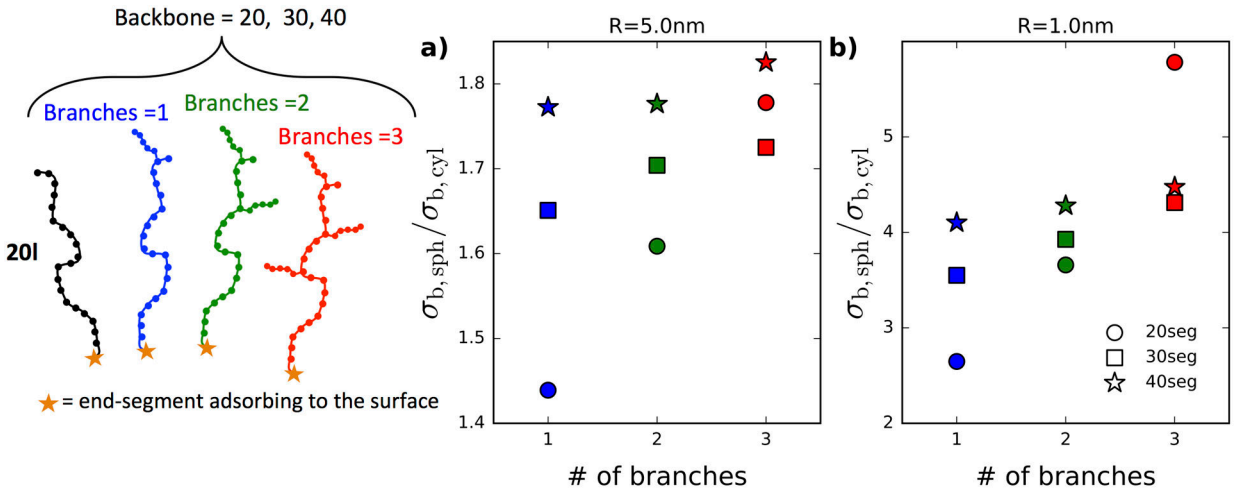

Figure 9:

Partition of the branched polymer between a sphere and a cylinder of radius 5 nm (panel **a**) and 1 nm (panel **b**). Polymer mixtures comprise a linear polymer of 20 monomers (20l) and a branched polymer with one, two, or three branches (in blue, green and red respectively) and backbone lengths of 20, 30, and 40 monomers (in circle, square, and star symbols respectively, see scheme on the left). All the cases are for a fixed bulk composition with $x_b^{bulk} = 0.9$.

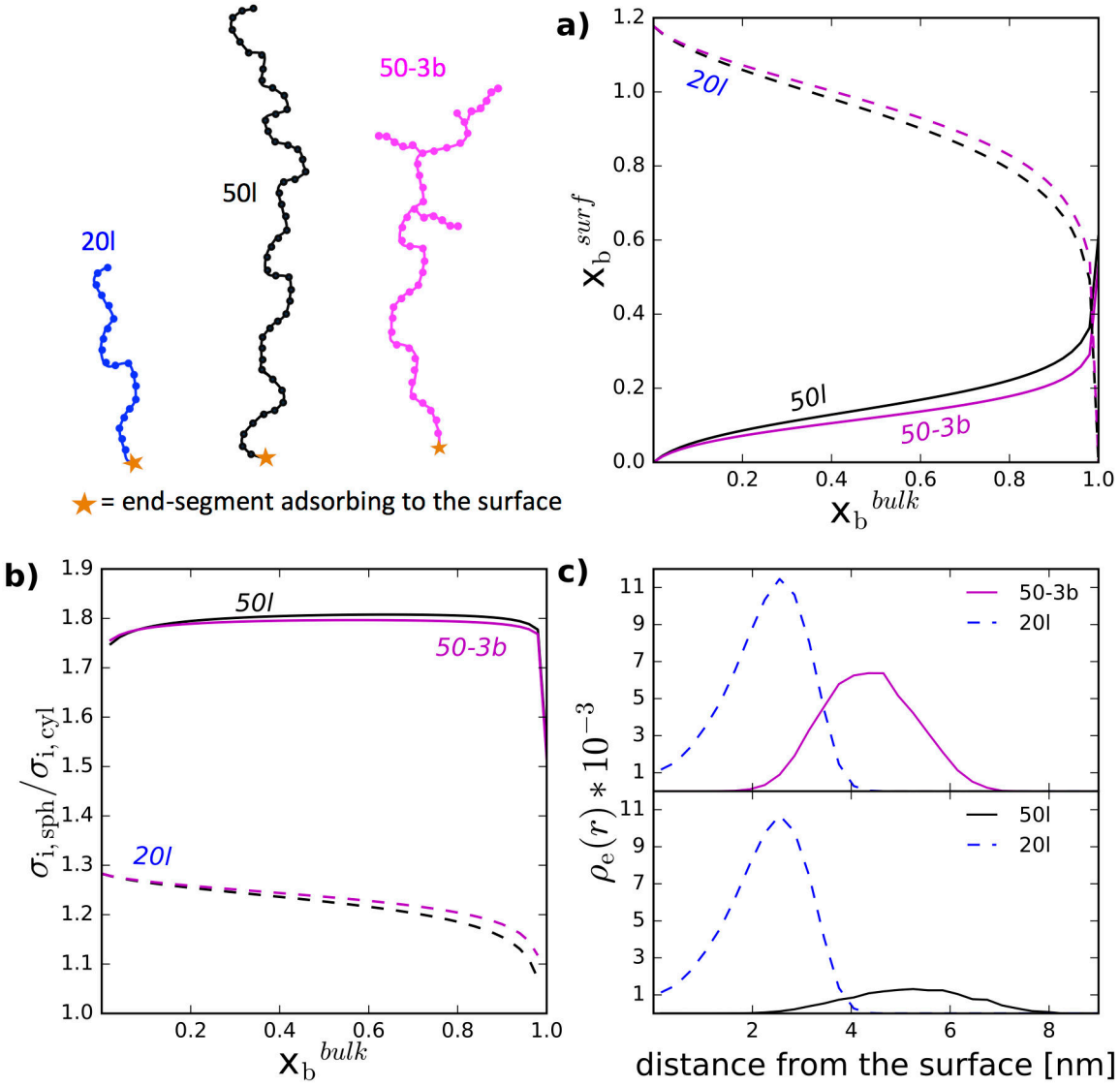

Figure 10:

Effect of the molecular topology on the competitive adsorption of binary mixtures. **a)** Surface density of adsorbed polymers as a function of the bulk molar fraction of the branched polymer. The full magenta and full black lines correspond to the 50l and 50–3b polymers respectively. Similarly, the dashed magenta and dashed black lines correspond to the 20l polymer in the 20l-50l and the 20l-(50–3b) mixtures respectively (see scheme on the upper left panel). Results correspond to a spherical surface of $R = 5$ nm. **b)** Partition of the linear and branched polymers between a sphere and a cylinder of 5 nm radius for the 20l-50l (magenta) and the 20l-(50–3b) (black) mixtures. **c)** Density of free ends as a function of the distance from the tethering surface for a spherical surface of $R = 5$ nm. All the cases are for a fixed bulk composition with $x_b^{bulk} = 0.9$. Lines and colors are indicated in the legend.

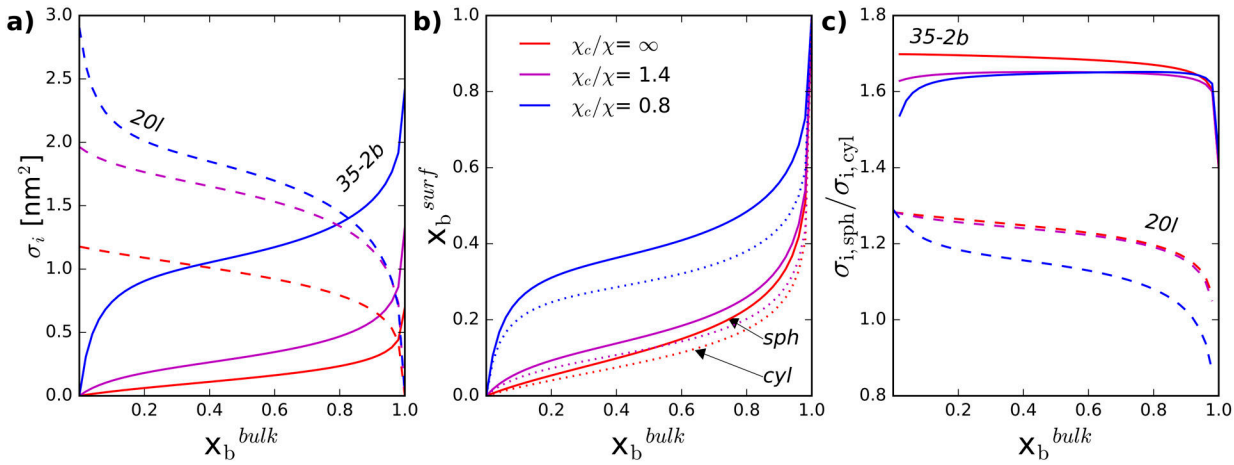

Figure 11:

Effect of solvent quality on the adsorption from polymer mixtures comprising a linear polymer of 20 monomers (20l) and a branched polymer with backbone length of 25 segments and 2 branches (35–2b). Red, magenta, and blue lines correspond to values of $\chi_c/\chi = \infty$, 1.4, and 0.833, respectively (see legend of panel b). **a)** Surface density of adsorbed linear (dashed lines) and branched (full lines) polymers as a function of the bulk molar fraction of the branched polymer for a spherical surface of R = 5nm. **b)** Molar fraction of the branched polymer adsorbed on the surface as a function of the bulk molar fraction of the branched polymer for spherical (full lines) and cylindrical (dotted lines) surfaces of R = 5nm. **c)** Partition of the linear (dashed line) and the branched (full line) polymer between a sphere and a cylinder of 5 nm radius as a function of the bulk molar fraction of the branched polymer.